A mechanism for the multidecadal modulation of ENSO teleconnection with Europe

Jorge López-Parages (1), Belén Rodríguez-Fonseca (1), Laurent Terray (2)

(1) *Departamento de Física de la Tierra, Astronomía y Astrofísica I (Geofísica y Meteorología). Instituto de Geociencias UCM-CSIC. Universidad Complutense de Madrid, Madrid, Spain.*

(2) *CERFACS/CNRS, Climate Modelling and Global Change Team, 42 avenue 14 Gaspard Coriolis, 31057 Toulouse, France.*

Corresponding author address: Jorge López-Parages. Departamento de Física de la Tierra, Astronomía y Astrofísica I, Facultad de C.C. Físicas. UCM, Pza de las Ciencias 28040-Madrid, Spain. parages@fis.ucm.es

Keywords: Atmospheric teleconnection, ENSO, European rainfall, Multidecadal Modulation.

0. Abstract

El Niño phenomenon is the main oceanic driver of the interannual atmospheric variability and a determinant source of predictability in the tropics and extratropics. Several studies have found a consistent and statistically significant impact of El Niño over the North Atlantic European Sector, which could lead to an improvement of the skill of current seasonal forecast systems over Europe. Nevertheless, this signal seems to be non-stationary in time and it could be modulated by the ocean at very low frequencies. Hence, the seasonal climate predictability based on El Niño could be variable and only effective for specific time periods. This study considers the multidecadal changes in the ocean mean state as a possible modulator of ENSO-European rainfall teleconnection at interannual timescales. A long control simulation of the CNRM-CM5 model is used to substantiate this hypothesis and to assess if it can be relevant to explain the non-stationary behavior seen in the 20th century. The model reproduces the leading rainfall mode over the Euro-Mediterranean region, and its non stationary link with El Niño. This teleconnection has been identified in coincidence with changes of the zonal mean flow at upper levels, which influence the propagation of the waves from the tropics to extratropics through the atmosphere and, hence, to explain the changing impact over Europe. However, the non-stationary impact observed along the 20th century could also be related to the observed changes in the interannual oceanic forcing signal itself. The results obtained suggest, for both hypotheses, an important role of the natural internal variability of the ocean at multidecadal timescales.

1. Introduction

The climate variability over the North Atlantic European Sector (NAES) is mainly linked to the North Atlantic Oscillation (NAO; Van Loon and Rogers 1978; Wallace and Gutzler 1981), which is characterized by a Sea Level Pressure (SLP) seesaw between the Azores high and the Icelandic low (Walker 1924). This fluctuation between subpolar and subtropical North Atlantic latitudes influences the stormtracks, and hence, the associated precipitation regime (Rodwell et al. 1999; Hurrell et al. 2003). Although the NAO is mainly associated with internal atmospheric variability, it is also influenced by changes in Sea Surface Temperature (SST), which could lead to predictability at seasonal to interannual time scales (Czaja and Frankignoul 1999; Hurrell et al. 2003). Several studies have found a consistent and statistically significant ENSO signal on the European climate (Fraedrich and Müller 1992; Moron and Plaut 2003). Interestingly, its low-level atmospheric pattern is similar to the one associated with the internal NAO (García-Serrano et al. 2010). In general, El Niño tends to be associated with a negative phase of the NAO (Brönnimann 2007). This raises the issue of a robust detection of the atmospheric response to ENSO as the forced response projects onto the leading mode of internal variability. Furthermore, an additional factor is that the influence of the NAO (Hilmer and Jung 2000; Lu and Greatbatch 2002; Vicente-Serrano and López-Moreno 2008) and ENSO (López-Parages and Rodríguez-Fonseca 2012; Greatbatch et al. 2004; Mariotti et al. 2002; Zanchettin et al. 2008) over the North Atlantic European climate, has not been stationary along the 20th century. Hence, the seasonal climate

predictability could be variable and only effective for specific time periods, contributing in that way to the poor skill of current seasonal forecast systems over Europe (Van Oldenborgh 2005).

A recent study of López-Parages & Rodríguez-Fonseca (2012, hereafter LPRF12) indicates, using observational data of rainfall, SLP and SST along the 20th century, that the leading mode of interannual rainfall in the European region is significantly correlated with El Niño during some particular decades whilst, in others, there is no link with any large scale oceanic pattern. The spatial structure of the associated SLP field was similar to the traditional NAO. However, to better determine the dynamical link, the study of upper atmospheric levels is crucial, as was demonstrated by Garcia Serrano et al. (2010). ENSO influence over NAES can take place through different mechanisms which could include the alteration of the thermally driven overturning atmospheric circulation (Wang 2002; Wang and Enfield 2003; Wang et al. 2004; Ruiz-Barradas et al. 2003), downstream propagation of Rossby waves, including or not the stratosphere (Hastenrath 2000; Cassou and Terray 2001b; Honda et al. 2001; Castanheira and Graf 2003; Ineson and Scaife 2008), or combinations of these mechanisms. The former occurs by the alteration of the Walker and Hadley circulations in relation to changes in the convection. The latter is explained through changes in the vorticity due to the meridional displacement of the flow at upper levels as a result of the divergence associated with the convection in the tropics. This vorticity disturbance triggers Rossby waves propagating over the extratropics and altering the atmospheric circulation over remote regions. In this way, a non-stationary impact of ENSO over Europe should be related to a non-stationary behavior of one (or both) of the previous mechanism. Recent studies have also found noticeable differences in the impacts of the two major ENSO patterns, Eastern and Central Pacific events (Kug et al. 2009; Kao and Yu 2009; Choi et al. 2011), the former being representative of the most intense El Niño events and the latter linked with the most intense La Niña ones (Dommenget et al. 2012). In this study non-Linear impacts of ENSO are not analyzed, each kind of episodes could be related to different non-stationary feature of the abovementioned mechanisms (An and Wang 1999, Fedorov and Philander 2000, An 2009; Choi et al. 2010; Yeh et al. 2011). A possible hypothesis that could explain the changing impact of ENSO over the NAES is associated with a modulation of the teleconnection by which the forcing signal is transmitted to the target area depending on the background state. Hence, an interesting issue to be explored here is the influence of oceanic low frequency variability modes, such as Atlantic Multidecadal Oscillation (AMO, Enfield et al. 2001), or Pacific Decadal Oscillation (PDO, Mantua et al. 1997), in the modulation of the atmospheric teleconnection mechanisms at interannual timescales. In this sense, LPRF12 found how the correlation between the leading rainfall mode in Europe and the anomalies over the Niño3.4 region evolves at multidecadal timescales in phase with AMO, and PDO, depending on the season considered. Building on these previous studies, the main questions we wish to address in the present work are as follows: 1) is there any SST multidecadal pattern, internal to the ocean, that could be able to modulate the ENSO teleconnection with Europe? 2) How does this SST pattern modulate the teleconnections? 3) What are the associated dynamical mechanisms? 4) Is there any preferred phase of these multidecadal SST modulating patterns for which the ENSO-Europe teleconnection is more efficient?

Therefore, the present study is mainly related to the non-stationary influence of ENSO over the NAES and how the internal variability of the slowly variant background state of the ocean can modulate this teleconnection.

The available literature suggests January to March as an appropriate season to study the ENSO influence over Europe (Brönnimann et al. 2007), being convenient to separate the weak ENSO-related circulation over the North Atlantic in early winter with the much stronger one during mid-late winter (Toniazzo and Scaife, 2006; Gouirand et al. 2007). Even in the North Pacific, the canonical Tropical Northern Hemisphere pattern (TNH, Mo and Livezey 1986; Barnston and Livezey 1987; Livezey and Mo 1987; Trenberth et al. 1998) related to ENSO is not completely established until January (Bladé et al. 2008). For these reasons this work is focused on the non-stationary ENSO-European rainfall teleconnection in late winter early spring, selecting the season February-March-April, according to LPRF12. A complete analysis cannot be carried out using only observations due to the shortness of the record and limited sampling of multidecadal SST modes. It is thus of interest to use a model approach where the non-stationary behavior could be assessed on multi-centennial simulations. To this aim, a long coupled simulation with constant pre-industrial forcing has been analyzed to complement the observational analysis. If the changes identified in the ENSO-European rainfall relationship along the 20th century could be reproduced only considering the internal variability of the climate system, it would suggest that the responsible mechanism of the non-stationary behavior is not necessarily related to anthropogenic changes.

The paper is organized as follows. We begin by presenting the data and methods used (section 2). In section 3 the covariability of European rainfall and tropical SSTs is analyzed for observations. The same analysis is applied to a long control simulation of the CMIP5-CM5 coupled model in section 4. In section 5, observed and modeled composites maps of different fields are compared to each other. Then, in section 6, some plausible hypotheses of the non-stationary features identified are presented and finally, in section 7, a brief summary is presented.

2. **Data and Methods**

This work is focused on the interannual precipitation over the Euro-Mediterranean region (iEMedR; 24 ºN-68ºN, 15ºW-35ºE), in late winter-early spring (February-March-April, FMA).

Two different observational databases have been used: University of Delaware rainfall data (Matsuura and Willmott, version 2.01, 2009, http://climate.geog.udel.edu/climate/html_pages/), and Global Precipitation Climatology Centre data (GPCC; Schneider et al. 2008). Both data are monthly climatology of precipitation spanning the whole 20th century and the beginning of the 21th century. They are land-only in coverage and are based on interpolated data from stations. Regarding the SST data, ERSSTv3 (Smith et al. 2008) from 1854 to present (2° x 2° lat long), and HadISST1 (Rayner et al. 2003) from 1870

to present (1°x 1° lat long) have been used. To pose a possible dynamical mechanisms and be able to compare it with the model outputs, atmospheric fields from the 20th Century Reanalysis V2 data provided by the NOAA/OAR/ESRL PSD, (Boulder, Colorado, USA; http://www.esrl.noaa.gov/psd/), have also been used.

The climate model data are provided by a long control coupled simulation (hereinafter PICTRL) of the CNRM-CM5 model (cf. Voldoire et al. 2013). This model includes the ARPEGE-Climat (v5.2) atmospheric model (1.4°x1.4°, 31 vertical levels, being 26 of them in the troposphere), the NEMO (v3.2) ocean model (ORCA1°, 42 vertical levels), the ISBA land surface scheme and the GELATO (v5) sea ice model coupled through the OASIS (v3) system. The PICTRL analyzed here is an 800 year long simulation where all external forcings (solar, volcanic and anthropogenic Greenhouse Gases and aerosols) are kept constant at their observed values of 1850.

Regarding the methodology, a Maximum Covariance Analysis (MCA, or Singular Value Decomposition; Bretherton et al. 1992) has been applied to identify the modes that explain the maximum covariance between the anomalous Euro-Mediterranean rainfall and tropical SST (20 ºN-20ºS). Each mode comprises two spatial structures (singular vectors), two time series (expansion coefficients; U and V for the predictor and predicted field respectively), and the covariance fraction, which is a measure of the percentage of covariability explained by each mode. The most common procedure when analyzing MCA results is to plot the projection of the predictor field (tropical SSTs here), and the field to predict (Euro-Mediterranean rainfall), on the standardized U, obtaining in that way the homogeneous and heterogeneous maps respectively. Along this study some composite maps also based on U have been obtained, being 1 standard deviation of U the threshold selected in PICTRL, and 0.75 standard deviation in observations. This difference in the threshold is considered to balance the number of cases selected in both, model and observations. These composites have been calculated to analyze the changes in the spatial patterns depending on the time period, and also to infer possible related dynamical mechanisms.

To retain only the interannual variability for all the fields analyzed here, periods lower than 7 years have been subtracted by applying a temporal filter based on a Discrete Fourier Transform. Looking for the stationarity of El Niño impact, different sliding window correlation analysis have been applied along the study, using 21 year as the reference window, for comparison with previous studies.

The correlation statistical significance has been determined by a non parametric approach using a Monte-Carlo test with 400 permutations. The spatial patterns significance has been also determined by non parametric approaches such as, Monte-Carlo test, or Wilcoxon-Mann-Whitney test (Wilks 2005).

3. Rainfall-SST covariability: Observational Results

As it was shown in LPRF12, the teleconnection between El Niño and the European rainfall leading mode of variability in late winter-early spring seems to be non-stationary on time, changing along the 20th century in phase with the Atlantic Multidecadal Oscillation (AMO). The leading EOF is shown in figure 1a, which is consistent with the ENSO signal over the European rainfall (Fraedrich and Müller 1992; Moron and Plaut 2003; Pozo-Vázquez et al. 2005a). In order to delve into the existence of this impact and to discard it as a statistical artifice, a time index based on this leading EOF has been used. This index has been calculated as the difference of area-average rainfall over Western Europe and Western Mediterranean region. These areas are two centers of actions of the leading EOF (black boxes in Figure 1a), and they do not coincide with those in the second and third modes of variability (see Figure A1 of supplementary material). Time correlation between the leading PC and the above-mentioned index is 0.83, which supports the absence of a mathematical artifact in the calculation of the leading EOF. The link with the equatorial SSTs is, moreover, non-stationary on time (Fig. 1b). Thus, strong correlations with the whole Indo-Pacific equatorial basin are positive from 1900's to 1940's and from 1960's to 1980's. However, for the years in between and, in the beginning of the 21th century, the correlations are weaker and of opposite sign. For the whole 20th century, the SST pattern coincides in sign in the Pacific and Indian oceans, while being opposite over the Maritime Continent. Although the magnitude of the correlation scores slightly differs between HadISST and ERSST (not shown), in both cases the maximum values are located over the Niño3.4 region, as in LPRF12. In agreement with Figure 1b, the Euro-Mediterranean rainfall PC1 and the Niño3.4 index (Fig. 1c) broadly correlate from 1900 to 1940 (0.47), and from 1965 to 1984 (0.42) approximately, while they are mainly anticorrelated from 1944 to 1964 (-0.23), and from 2003 to 2008 (-0.73).

The previous results reinforce those of LPRF12 and show how, although the dipolar rainfall pattern identified as EOF1 is present along the whole observational period, it might be enhanced and potentially predictable when its relation with tropical SSTs is stronger. It also shows that this link mainly takes place in the 20th century during negative phases of AMO. As it was indicated in Sect. 2, MCA is a discriminant analysis tool which is very useful for finding coupled patterns in climate data and, thus, for determining the most frequent predictors for a variable to predict. With the purpose of confirming the changing coupling between rainfall and SST, two different MCA analyses linking the Euro-Mediterranean rainfall and the tropical SST have been performed selecting two different samples according to the changing relationship previously identified. The first sample covers the periods 1944-1964, and 2003-2008, which correspond to the years with negative correlations between rainfall and Niño3.4 (Fig. 1c). The second sample (1900-1940 and 1965-1984) corresponds to the periods with positive correlations between the same indices. Hereinafter these periods will be referred as N (Negative correlations) and P (Positive correlations) periods respectively.

The leading mode of covariability for the P period (Fig. 2b, d), which explains 31.1% (28.3% for ERSST) of the total covariance, resembles the link identified in LPRF12 (see Figure 1 of LPRF12). The spatial correlation between the rainfall anomalous pattern obtained in LPRF12 and that obtained here from the MCA_P is 0.88 (0.85 for ERSST). On the other hand, for N periods (Fig. 2a, c), the leading mode, which

in this case explains 23.3% (21.6% for ERSST) of the total covariance, shows a similar SST pattern than in P periods, but in relation to a completely different rainfall pattern. The spatial correlation between the rainfall pattern from LPRF12 and that obtained here from the MCA_N is -0.61 (-0.59 for ERSST). These rainfall maps obtained for each MCA broadly coincide with the simple regression of rainfall anomalies on the Nino3.4 index (see Figure A2 of supplementary material) for the selected periods. Although the tropical SSTs for both MCAs are similar, it is worth to highlight the enhanced signal identified in P over the Tropical North Atlantic (TNA) and the Maritime continent regions. This issue will be discussed in section 5.

As the observed changing link between rainfall and tropical Pacific SSTs appears in phase with the AMO, and this oceanic mode is internal to the ocean, a long coupled control simulation has been used to test if this non-stationary relationship could be reproduced by the model multidecadal internal variability without any changes in external forcing.

4. Model performance

It is first necessary to assess the ability of the model to reproduce the leading mode of observed interannual rainfall variability. The observed and simulated modes present a similar spatial pattern (Fig. 3a), with significant scores in central Europe, including the British Islands, and the surrounding areas of the Baltic Sea. These anomalies are opposite in sign to those over the Mediterranean region, the northwestern Africa, and the north of Scandinavia. This leading rainfall mode can be described through the same simple index previously used in observations (see black boxes in Figure 1a). In this case PC1 is correlated at 0.89 with the defined index. Slight differences with observational EOF1 are found in the intensity and location of the centers of action, and in the decrease of the explained variance by the leading mode (19.2% in observations and 14.4% in PICTRL). This fact is probably explained by the large difference in the number of years analyzed in observations (109 years) and PICTRL (800 years). In spite of this decrease in the explained variance, the leading mode of PICTRL is well separated to the second one according to the criteria of North et al. (1982). Looking for the stationarity of the rainfall mode, 21-yr window sliding correlations have been calculated here (Fig. 3b) between the rainfall leading PC and the Niño3.4 index, indicating a quasi-cyclic behavior in the relationship and, as a consequence, periods with positive, negative, or even no correlation. This time evolution is highly similar to the leading PC of the low frequency SST variability of the model (Fig. 3b). PICTRL, which is a long control simulation, is a useful tool to assess the time evolution identified in the moving correlations (see also Figure A3) and its possible connection with multidecadal modes such as AMO, as was proposed in LPRF12.

As in the observations, two different, and opposite, relationships emerge between rainfall and El Niño along the PICTRL, suggesting the existence of different underlying dynamics that alternate at multidecadal timescales. To further analyze this issue, periods with negative (N, 169 years) and positive (P, 137 years) significant correlations have been analyzed separately.

MCA analysis between model anomalous rainfall and tropical SSTs has been performed for P and N. The leading modes of covariability account for 20.0% and 21.9% of the total variance, respectively. The resultant oceanic patterns (Fig. 4c, d) resemble the ones obtained in observations (Fig. 2c, d). However, unlike it happens in observations, the model ENSO signal is almost the same in P and N, putting forward how in PICTRL, the interannual SST forcing seems to be stationary. Nevertheless, its impact on rainfall is opposite in P and N periods over central Europe and the Mediterranean region. The spatial correlation between the rainfall patterns obtained for each period and the EOF1 for the whole PICTRL (Fig. 3a) are -0.90 and 0.71 for N and P respectively, reinforcing the idea of a changing impact over the Euro-Mediterranean area for the same tropical forcing.

In the next section the atmospheric variables related to the leading modes of covariability obtained for N and P periods are analyzed in order to infer different hypothesis for the dynamical mechanisms involved in the teleconnection.

5. **Dynamical mechanisms in the teleconnection**

ENSO influence over NAE sector can take place through different mechanisms which could include the alteration of the thermally driven overturning atmospheric circulation (Wang 2002; Wang and Enfield 2003; Wang et al. 2004; Ruiz-Barradas et al. 2003), downstream propagation of Rossby waves, including or not the stratosphere (Hastenrath 2000; Cassou and Terray 2001b; Honda et al. 2001; Castanheira and Graf 2003; Ineson and Scaife 2008), or combinations of these mechanisms. The former occurs by the alteration of the Walker and Hadley circulations in relation to changes in the convection. The latter is explained through changes in the vorticity due to the meridional displacement of the flow at upper levels as a result of the divergence associated with the convection in the tropics. This vorticity disturbance triggers Rossby waves propagating over the extratropics and altering the atmospheric circulation over remote regions.

In this section, several composites maps have been calculated for each time period and for different variables involved in the above mentioned mechanisms. The expansion coefficient of tropical SSTs (hereinafter U) from each MCA has been used to perform "high minus low" composites maps as the difference between events for which U is greater than (high events), or lower than (low events) an imposed threshold (see section 2).

The observational results are represented in Figure 5 for N and P periods. In both cases, a warming (cooling) in El Niño and a extratropical horseshoe pattern over the North Pacific (Fig. 5a, b) appears in relation to an anomalous upper level divergence (convergence) over the central equatorial basin (Fig. 5c, d) and a weakening (strengthening) of the subtropical Pacific anticyclone. However, the tropical divergence together with its rotational response is clearly enhanced in P periods (Fig. 5c, d), as a consequence of the stronger El Niño amplitude in decades in which the north Atlantic is cooler than the

south Atlantic, as it happens in P periods (Dong et al. 2006; Zhang et al. 2011). In agreement with Wang (2002), El Niño signal over the Pacific appears together with a heating in the Tropical North Atlantic (TNA), in association with a weakening of the Azores high (Fig. 5f). The connection takes place through changes in the Walker and Hadley circulations, as it can be seen by the Atlantic anomalous upper level convergence over South America and divergence over the TNA region (Fig. 5d). As the TNA region highly influences the ENSO-related atmospheric response over the NAE sector (Mathieu et al. 2004), its stronger signal for selected P periods, a time period with a stronger relation of El Niño with the rest of the tropical basins (Losada et al. 2010b, 2012), could explain the non stationary impact of El Niño over the European climate. This feature could, however, be also associated with the multidecadal variability of the Atlantic Warm Pool that is known to vary in phase with the AMO (Wang et al. 2008b). In general, the significant differences identified over the extratropical Atlantic and Pacific suggest a changing influence of the atmosphere on the underlying ocean (Fig. 5a, b). Regarding the tropical Indo-Pacific basin, warmer SSTs are observed in P from the Maritime continent to the Japan Islands. Thus, Rossby Wave Sources over these regions might be intensified in response to the warmer ocean. Moreover, in P as well, a stronger longitudinal gradient seems to take place over the west equatorial Pacific, in agreement with Meng et al. (2012), who have related it to a weakening of the Walker Circulation in association with a warmer Indian ocean. As a consequence of the changes in the tropical upper level divergence, an anomalous rotational circulation appears to balance the variation in the planetary vorticity to preserve the potential vorticity. For both, N and P periods, two twin anticyclones straddling the equator over the tropical Pacific reflect the typical Gill-type atmospheric response to equatorial anomalous heating (Gill 1980). However, only for P periods, the wavetrain propagating from the tropical Pacific resembles the well known TNH pattern. Moreover, a strong negative center of action also appears in P over Scandinavia. The whole quadrupolar atmospheric pattern over the North Atlantic-European sector has a quasi-barotropic structure (Fig. 5d, f) except for the Iberian Peninsula center that is not significant at surface levels. This configuration is coherent with the leading mode of upper level streamfunction in mid-winter obtained by García-Serrano et al. (2010), and related to El Niño extratropical rotational atmospheric response. Complementary to that study, in which the stationary behavior is not discussed, this spatial structure (see Figures 1 and 3 of that paper) is found here just for selected P periods. The centre of action located over Scandinavia in P might be due to a split of the ENSO wavetrain originated in the tropical Pacific, as was suggested by García-Serrano et al. (2010) for January-February. The appearance of this pattern over the North Atlantic (Fig. 5d, f), and the role of low frequency changes in the ocean on its nonstationary behavior, will be further analyzed below.

For N decades, however, in agreement with a weaker heating at surface and a weaker divergent flow at upper levels, the TNH pattern weakens and the resultant configuration over North-Atlantic Europe (Fig. 5c) is different. At surface (Fig. 5e), the strong center of action located over the North Sea resembles an atmospheric blocking pattern. Thus, it seems that these blocking structures could be favored in N periods, in agreement with recent results putting forward an enhancement of the frequency of blocking events under positive phases of the AMO (Häkkinen et al. 2011).

342 Model results are represented in Figure 6 for N and P periods. Contrary to the observations, the SST
343 patterns and the associated perturbation of the divergent flow are highly similar to each other (Fig. 6a, b).
344 The stronger influence in P of the atmosphere on the extratropical Atlantic and Pacific basins is, however,
345 well reproduced by the model. The significant divergence signal over the North Atlantic, which is found
346 in PICTRL for both N and P, resembles the response found just for P in observations. The significant
347 upper level convergence over the equatorial Atlantic for PICTRL (Fig. 6c, d) appears in relation to an
348 underlying warming (Fig. 6a, b), indicating the dominant influence of the remote warming in comparison
349 with the local warming (which would induce divergence at upper levels). A significant velocity potential
350 signal is also identified in PICTRL over the Indian Ocean, being slightly stronger for P periods. A
351 striking feature is that these similar divergent responses for P and N are related to different rotational
352 responses over the NAES (Fig. 6c, d). Over this region, the wave pattern at upper levels seems to
353 significantly reach the European continent in P, the response being broadly the same as the one identified
354 in observations at surface (Fig. 5f, 6f) and upper levels (Fig. 5d, 6d). Conversely, in N, the North Atlantic
355 region is less perturbed by the TNH pattern and a dipolar configuration emerges at surface (Fig. 6e),
356 resembling an internally driven NAO configuration and not the blocking pattern that appears in the
357 observations (Fig. 5e).
358
359 Previous works have documented changes in the location of the actions centers of the NAO along the 20th
360 century (Hilmer and Jung 2000; Lu and Greatbatch 2002, Vicente-Serrano and López-Moreno 2008).
361 Thus, our results could suggest an additional non-stationary external forcing over the NAES that could
362 contribute to the documented changes in the observed NAO structure.
363
364 In agreement with the above mentioned results, it seems that the model is able to reproduce the observed
365 impact of ENSO over the Northern Hemisphere and the Euro-Mediterranean region, at least, for selected
366 periods (P). However, although the mechanism could be related to the Walker-Hadley atmospheric bridge
367 and the TNH pattern, a different extratropical response occurs in relation to almost the same tropical
368 heating in PICTRL for N periods (see Figure A4 of supplementary material). At this point a question
369 emerges: if the forcing from the tropical Pacific SSTs is considered stationary in PICTRL, why the impact
370 over the European rainfall is so different? A plausible explanation is that the zonal mean flow at upper
371 levels, which influences the propagation of Rossby waves (Hoskins and Ambrizzi 1993), changes due to
372 variations of the low-frequency oceanic forcing. This issue is analyzed in the next section.
373
374 **6. Contribution of mean state changes to the interannual teleconnection**
375
376 As it has been previously shown, tropical heating associated with El Niño is similar in N and P periods
377 for PICTRL, so the distinct signals identified for each kind of period could reasonably be attributed to
378 variations in the mean state. The characteristics of a control simulation make easier the inference of the
379 role of low frequency SST internal variability because external forcings are constant and thus not
380 considered. According to the results obtained in PICTRL, the changes in El Niño teleconnection observed

over the North Atlantic and the Euro-Mediterranean region could be explained through changes in the internal mean state (not forced by the GW).

The rotational flow at upper levels previously plotted in Figures 5d, 6c and 6d is presented in Figure 7 in a north polar stereographic projection, identifying a similar configuration for those periods with a significant divergence flow signal associated with ENSO (P and N in PICTRL and P in observations). Nevertheless, the TNH pattern over the NAE sector is clearly weaken in PICTRL for N periods (Fig.7a), while in P (Fig.7b), the configuration over the North Atlantic is significantly stronger and highly similar with the observations (Fig. 7c). According to the basic Rossby Wave Theory proposed by Hoskins and Ambrizzi (1993), the planetary waves are always refracted towards latitudes with higher Rossby wavenumbers (Ks). As a consequence, positive anomalies of Ks indicate regions with a reinforced waveguide. Thus, the northward displacement of the Indo-Pacific jet in P (Fig. 8a), and its related Rossby waveguide (Fig. 8b), over the North Pacific, can explain the enhanced propagation of the disturbances to higher latitudes for P periods in the model. Hence, a stronger ENSO-related rotational atmospheric pattern over the NAES (Garcia-Serrano et al. 2010) is identified (Fig 7b). This difference could explain the non-stationary impact on rainfall between P and N periods in the model. The rotational flow configuration shown in Figure 7 is also coherent with a remote displacement of the disturbances along the northern hemisphere due to the above-mentioned waveguide effect of the zonal mean flow (Hoskins and Karoly 1981; Branstator 1992, Hsu and Lin 1992; Hoskins and Ambrizzi 1993; Ambrizzi et al. 1995; Branstator 2002). Thus, it seems that a more efficient waveguide effect and so, a stronger hemispheric response, could also contribute in P to the above mentioned ENSO-related rotational impact over the North Atlantic.

These changes in the zonal mean flow are related to the underlying ocean multidecadal variability (Fig. 8c), which signal appears significant over the North Pacific and Atlantic basins, resembling typical multidecadal variability patterns associated with the well known PDO (Mantua et al. 1997) and AMO modes (Knight et al. 2005). As the jet streams are partially caused by the meridional temperature gradient in the earth's atmosphere, a significant change in their location could be expected if the underlying ocean temperature varies along the time. Thus, the non-stationary impact over the NAE sector identified in PICTRL could ultimately be explained by changes in the zonal mean flow forced by the slowly variant component of the ocean.

The observational results point to the same impact over the NAES for P periods, in agreement with Lopez-Parages and Rodríguez-Fonseca (2012). Some slight differences appear, however, in the location of the extratropical centers of action in PICTRL (Fig. 7b) and observations (Fig. 7c), with a westward displacement in the former case. This fact could be explained by both, the more westerly location of the forcing region (see Fig. 5, 6), and the less elongated Indo-Pacific jet (Fig. 7b, c), in the model.

7. Summary

In this paper the link between the leading mode of interannual anomalous rainfall in the Euro Mediterranean region and El Niño found in Lopez-Parages and Rodriguez Fonseca (2012) has been further investigated using a long control simulation of the CNRM-CM5 model. The aim of the study is to find if the observed multidecadal modulations of ENSO teleconnections with Europe can be reproduced by the internal low frequency variability of the coupled system without invoking any role for anthropogenic forcing. The study is focused on the late-winter early spring, which is a characteristic season in which ENSO exerts an influence over North Atlantic and Europe (Brönnimann 2007; Zhang et al. 2011). The working hypothesis is that ENSO teleconnections are not stationary and the multidecadal natural variability of the ocean acts as a modulator, in agreement with the results of Lopez-Parages and Rodriguez-Fonseca (2012).

In this way, the correlation between the observed Euro-Mediterranean rainfall and ENSO is stronger in some decades (P) than in others (N). For P, broadly in coincidence with 20th century negative phases of AMO, an increase of rainfall over central Europe and a decrease over the Mediterranean area occurs jointly with a warming over the tropical Pacific and Indian basins, and a cooling over the Maritime continent. As the correlations obtained evolve in phase with the AMO, which is a natural internal variability mode of the ocean, a long coupled control simulation has been considered as a useful dataset to analyze the internal effect in the observed modulation.

In particular, the CNRM-CM5 model long control simulation has been used. This model reproduces the observed leading rainfall mode and its non-stationary link with El Niño, confirming in this way that the natural variability has an effect in modulating the impacts of El Niño in the extratropical North Atlantic region.

In the above-mentioned P periods two dynamical mechanisms are contributing to the ENSO teleconnection. Thus, alteration of the thermally driven direct circulation (Wang et. al 2002), and the ENSO related rotational North Atlantic mode (Garcia-Serrano et al. 2011), significantly affect the surface European rainfall in both, model and observations. The resultant configuration over the NAE sector has been previously associated with a non-stationary forcing from the tropics (Greatbatch et al. 2004), but also with a teleconnection pathway via the stratosphere (Ineson and Scaife 2008). In the latter work it is argued that the response over the NAES in late winter is explained by the occurrence of sudden stratospheric warming's, and so, a good representation of the stratosphere become crucial. Here, the same impact has been reproduced by a model which do not fully represent stratospheres processes ("low-top model"). Then, although the stratosphere could play also an important role, the teleconnection could be reproduced through tropospheric mechanism if the non-stationary features are considered. Nevertheless, this does not exclude a possible significant role for the stratosphere that could be analyzed in a similar setup with high-top models.

The ENSO related rotational flow impact is modulated, in PICTRL, by changes in the zonal mean flow at upper levels forced by the ocean. Hence, the surface signal over the NAES changes as well, resembling in

N periods a negative phase of the NAO. The observed N periods, coinciding with positive phases of the AMO, are characterized by a weakening of the ENSO signal. As a consequence, the previously commented mechanisms are also weakened and, an atmospheric blocking pattern appears in relation to an El Niño signal over the tropical Pacific. This link between ENSO and the enhanced frequency of blocking events under positive phase of AMO (Häkkinen et al. 2011) should be further investigated in the future.

Although this study is focused on late winter and early spring, non stationarities modulated at multidecadal timescales takes place from autumn to spring (see Fig. 2 of LPRF12). Thus, similar changes in the zonal mean flow forced by the ocean could also explain the changing impact identified in these seasons. This seasonal time difference in the nonstationary ENSO-NAES teleconnection is a task to be further research in future works.

Our results thus point to an important role (although not unique) of the multidecadal changes in the zonal flow forced by natural internal oceanic variability, in the modulation of El Niño effect on the European rainfall. As a fraction of the oceanic variability is linked to the Atlantic Meridional Overturning Circulation that is projected to weaken in the 21st century, it is possible that the interaction between El Niño and Europe change again in the next decades. Another explanation to the nonstationary impact of the same ENSO signal over the NAES could be related to a changing SSTs background state of the tropical Pacific, which in turn could be also forced by the Atlantic Ocean (Sutton and Hodson 2007). To get further insight into these issues, and to investigate nonlinear responses, sensitivity experiments with General Circulation Models (GCMs) should be done in the future.

Acknowledgments: We are indebted to CERFACS for providing the CNRM-CM5 control simulation, which has made possible this study. We thank to the University of Delaware, GPCC, NOAA, and the UK Met-Office for the provided data. The study has been partially supported by the National Spanish Projects: TRACS (CGL2009-10285) and MULCLIVAR (CGL2012-38923-C02-01). JLP also thanks the FPI grant BES-2010-042234 of the Ministerio de Economía y Competitividad of Spanish Goverment.
We would like to thank the anonymous reviewers for their helpful comments, which greatly helped to improve the manuscript.

References

An, SI (2009) A review of interdecadal changes in the nonlinearity of the El Niño-Southern Oscillation. Theoretical and Applied Climatology, 97(1-2), 29–40. doi:10.1007/s00704-008-0071-z

Ambrizzi T, Hoskins BJ,Hsu HH, (1995) Rossby wave propagation and teleconnection patterns in the austral winter. J. Atmos. Sci., 52, 3661-3672

An SI, Wang B (1999) Interdecadal Change of the Structure of the ENSO Mode and Its Impact on the ENSO Frequency. J. Clim.., 13, 2044-2056

Barnston, AG, Livezey RE, (1987) Classification, seasonality, and persistence of low-frequency atmospheric circulation patterns. Mon. Wea. Rev., 115, 1083–1126.

Bladé I, Newman M, Alexander M, Scott J (2008) The Late Fall Extratropical Response to ENSO: Sensitivity to Coupling and Convection in the Tropical West Pacific. J. Clim., 21, 6101-6118

Branstator G, (1992) The maintenance of low-frequency atmospheric anomalies. J. Atmos. Sci., 49, 1924–1946.

Branstator G (2002) Circumglobal Teleconnections, the Jet Stream Waveguide, and the North Atlantic Oscillation. J. Clim., 15(14), 1893–1910. doi:10.1175/1520-0442(2002)015<1893:CTTJSW>2.0.CO;2.

Bretherton C.S., C. Smith, J. W. (1992) An Intercomparison of Methods for Finding Coupled Patterns in Climate Data. J. Climate, 5(6), 541–560. doi:http://dx.doi.org/10.1175/1520-0442(1992)005<0541:AIOMFF>2.0.CO;2

Brönnimann, S (2007) Impact of El Niño–Southern Oscillation on European climate, Rev. Geophys., 45, RG3003, doi:10.1029/2006RG000199.

Cassou, C., Terray L (2001b) Oceanic forcing of the winter- time low-frequency atmospheric variability in the North Atlantic European sector: A study with the ARPEGE model, J. Climate., 14, 4266–4291.

Castanheira JM, Graf HF (2003) North Pacific–North Atlantic relationships under stratospheric control?, J. Geophys. Res., 108(D1), 4036, doi:10.1029/2002JD002754.

Choi J, Kug SAJ, Nin E (2011) The role of mean state on changes in El Nino's flavor, 1205–1215. doi:10.1007/s00382-010-0912-1

Czaja, A, Frankignoul, C (1999) Influence of the North Atlantic SST on the atmospheric circulation. Geophys. Res. Lett. 26(19), 2969–2972. doi:10.1029/1999GL900613

Dommenget D, Bayr T, Frauen C (2012) Analysis of the non-linearity in the pattern and time evolution of El Niño southern oscillation. Clim. Dyn., 40(11-12), 2825–2847. doi:10.1007/s00382-012-1475-0

536 Dong B, Sutton RT, Scaife AA (2006) Multidecadal modulation of El Niño–Southern Oscillation
537 (ENSO) variance by Atlantic Ocean sea surface temperatures, Geophys. Res. Lett., 33, L08705,
538 doi:10.1029/ 2006GL025766.
539
540 Enfield DB, Mestas Nuñez AM, Trimble PJ (2001) The Atlantic Multidecadal Oscillation and its relation
541 to rainfall and river flows in the continental U.S. Geophys. Res. Lett., 28(10), 2077.
542 doi:10.1029/2000GL012745
543
544 Fedorov AV (2000) Is El Nino Changing? Science, 288(5473), 1997–2002.
545 doi:10.1126/science.288.5473.1997
546
547 Fraedrich K, Müller K (1992) Climate anomalies in Europe associated with ENSO extremes, Int. J.
548 Climatol., 12, 25 – 31, doi: 10.1002/joc.3370120104
549
550 García-Serrano J, Rodríguez-Fonseca B, Bladé I, Zurita-Gotor P, Cámara A (2010) Rotational
551 atmospheric circulation during North Atlantic-European winter: the influence of ENSO. Clim. Dyn.,
552 37(9-10), 1727–1743. doi:10.1007/s00382-010-0968-y
553
554 Gill AE (1980) Some simple solutions for heat-induced tropical circulations. Q. J. R. Meteorol. Soc. 106:
555 447–462
556
557 Gouirand I, Moron V, Zorita E (2007) Teleconnections between ENSO and North Atlantic in an ECHO-G
558 simulation of the 1000–1990 period. Geophys. Res. Lett., 34(6), doi: 10.1029/2006GL028852
559
560 Greatbatch RJ, Lu J, Peterson KA (2004) Nonstationary impact of ENSO on Euro-Atlantic winter
561 climate. Geophys. Res. Lett., 31, L02208, doi:10.1029/2003GL018542
562
563 Häkkinen S, Rhines PB, Worthen DL (2001) Atmospheric Blocking and Atlantic Multidecadal Ocean
564 Variability. Science 4, November 2011: 334 (6056), 655-659. [DOI:10.1126/science.1205683]
565
566 Hastenrath S (2003) Upper-air circulation of the Southern Oscillation from the NCEP-NCAR reanalysis,
567 Meteorol. Atmos. Phys., 83, 51–65.
568
569 Hilmer, M, Jung, T (2000). Evidence for a recent change in the link between theNorth Atlantic
570 Oscillation and Arctic Sea ice export. Geophys. Res. Lett., 27(7), 989–992. doi:10.1029/1999GL010944.
571
572 Honda M,Nakamura H, Ukita J, Kousaka I,Takeuchi K (2001) Interannual seesaw between the Aleutian
573 and Icelandic lows, part I: Seasonal dependence and life cycle, J. Climate., 14, 1029–1041.

574
575 Hoskins BJ, Ambrizzi T (1993) Rossby wave propagation on a realistic longitudinally varying flow.
576 Atmos. Sci., 50, 1661-1671.
577
578 Hoskins BJ, Karoly K (1981) The steady response of a spherical atmosphere to thermal and orographic
579 forcing. J. Atmos. Sci. 38:1179–1196.
580
581 Hsu HH., Lin SH (1992) Global teleconnections in the 250-mb streamfunction field during the northern
582 hemisphere winter. Mon. Wea. Rev., 120, 1169-1190.
583
584 Hurrell JW, Kushnir Y, Ottersen G, Visbeck M (2003) An overview of the North Atlantic Oscillation, in
585 The North Atlantic Oscillation: Climatic Significance and Environmental Impact, Geophys. Monogr. Ser.,
586 vol. 134, edited by J. W. Hurrell et al., pp. 1–35, AGU, Washington, D. C., doi:10.1029/134GM01.
587
588 Ineson S, Scaife AA (2008) The role of the stratosphere in the European climate response to El
589 Niño.Nature Geoscience, 2(1), 32–36. doi:10.1038/ngeo381.
590
591 Kao HY, Yu JY (2009) Contrasting Eastern-Pacific and Central-Pacific Types of ENSO. J. Clim., 22(3),
592 615–632. doi:10.1175/2008JCLI2309.1
593
594 Knight JR, Allan RJ, Folland CK, Vellinga M, Mann ME (2005) A signature of persistent natural
595 thermohaline circulation cycles in observed climate. Geophys. Res. Lett. 32. doi:10.1029/2005
596 GL024233.
597
598 Kug JS, Jin FF, An SI (2009) Two Types of El Niño Events: Cold Tongue El Niño and Warm Pool El
599 Niño. J. Clim., 22(6), 1499–1515. doi:10.1175/2008JCLI2624.1
600
601 Livezey RE, Mo KC (1987) Tropical-extratropical teleconnections during the Northern Hemisphere
602 winter. Part II: Relationships between monthly mean Northern Hemisphere circulation patterns and
603 proxies for tropical convection. Mon. Wea. Rev., 115, 3115-3132.
604
605 López-Parages J, Rodríguez-Fonseca B (2012) Multidecadal modulation of El Niño influence on the
606 Euro-Mediterranean rainfall. Geophys. Res. Lett., 39(2), doi:10.1029/2011GL050049.
607
608 Losada T, Rodríguez-Fonseca B, Polo I, Janicot S, Gervois S, Chauvin F, Ruti P (2010b) Tropical
609 response to the Atlantic Equatorial mode: AGCM multimodel approach. Clim. Dyn. 5: 45-52.
610

611 Losada T, Rodríguez-Fonseca B, Mohino E, Bader J, Janicot S, Mechoso CR(2012) Tropical SST and
612 Sahel rainfall: A non-stationary relationship. Geophys. Res. Lett., 39, L12705. Doi:
613 10.1029/2012GL052423.
614
615 Lu J, Greatbatch RJ (2002) The changing relationship between the NAO and northern hemisphere climate
616 variability, 29(7), 1–4. doi:10.1029/2001GL014052.
617
618 Mantua NJ, Hare SR, Zhang Y., Wallace JM, Francis RC (1997) A Pacific interdecadal climate
619 oscillation with impacts on salmon production. Bull. Amer. Meteor. Soc., 78, 1069–1079
620
621 Mariotti A, Zeng N, Lau KM (2002) Euro-Mediterranean rainfall and ENSO: A seasonally varying
622 relationship, Geophys. Res. Lett., 29(12), 1621, doi:10.1029/2001GL014248.
623
624 Mathieu PP, Sutton RT, Dong B, Collins M(2004) Predictability of Winter Climate over the North
625 Atlantic European Region during ENSO Events, 17(1996), 1953–1974.
626 doi:http://dx.doi.org/10.1175/1520-0442(2004)017<1953:POWCOT>2.0.CO;2.
627
628 Matsuura K,Willmott CJ, Terrestrial Precipitation (2009) 1900-2008 Gridded Monthly Time Series
629 version 2.01, http://climate.geog.udel.edu/climate/html_pages/
630
631 Meng Q, Latif M, Park W, Keenlyside NS, Semenov VA, Martin T (2012) Twentieth century Walker
632 Circulation change: data analysis and model experiments. Clim. Dyn. 38, 1757-1773. DOI
633 10.1007/s00382-011-1047-8
634
635 Mo KC,Livezey RE, (1986) Tropical-extratropical geopotential height teleconnections during the
636 Northern Hemisphere winter. Mon. Wea. Rev., 114, 2488- 2515.
637
638 Moron M, Plaut G (2003) The impact of El Niño Southern Oscillation upon weather regimes over Europe
639 and the North Atlantic boreal winter, Int. J. Climatol., 23, 363 – 379, doi:10.1002/joc.890
640
641 North GR, Bell TL, Cahalan RF, Moeng FJ (1982) Sampling errors in the estimation of empirical
642 orthogonal functions, Mon. Weather Rev., 110, 699–706, doi:10.1175/1520-
643 0493(1982)110<0699:SEITEO> 2.0.CO;2.
644
645 Pozo-Vazquez, D, Gomiz-Fortis SR, Tovar-Pescador J, Esteban-Parra MJ, Castro-Diez Y (2005) El Niño-
646 southern oscillation events and associated European winter precipitation anomalies. Int. J. Climatol.,
647 25(1), 17–31. doi:10.1002/joc.1097.
648

649 Rayner NA, Parker DE, Horton EB, Folland CK, Alexander L V, Rowell DP, Kent EC, Kaplan A (2003)
650 Global analyses of sea surface temperature, sea ice, and night marine air temperature since the late
651 nineteenth century, J. Geophys. Res., 108(D14), 4407, doi:10.1029/ 2002JD002670.
652
653 Rodwell MJ, Rowell DP, Folland CK (1999) Oceanic forcing of the wintertime North Atlantic oscillation
654 and climate variability of northern Europe, Nature, 10, 1635–1647.
655
656 Ruiz-Barradas A, Carton JA, Nigam S (2003) Role of the atmosphere in climate variability of the tropical
657 Atlantic, J. Clim., 16, 2052–2065.
658
659 Schneider U. et al. (2008) Global Precipitation Analysis Products of the GPCC, Global Precip. Climatol.
660 Cent., Offenbach, Germany.
661
662 Smith TM, Reynolds RW, Peterson TC, Lawrimore J (2008) Improvements to NOAA's historical merged
663 land-ocean surface temper- ature analysis (1880–2006), J. Clim., 21, 2283–2296, doi:10.1175/
664 2007JCLI2100.1.
665
666 Sutton RT, Hodson DLR (2007) Climate response to basin-scale warming and cooling of the North
667 Atlantic Ocean, J. Clim.., 20, 891–907, doi:10.1175/JCLI4038.1.
668
669 Toniazzo T, Scaife A (2006) The influence of ENSO on winter North Atlantic climate. Geophys. Res.
670 Lett., 33(24), doi: 10.1029/2006GL027881.
671
672 Trenberth KE, Branstator GW, Karoly D, Kumar A, Lau NC, Ropelewski C (1998) Progress during
673 TOGA in understanding and modeling global teleconnections associated with tropical sea surface
674 temperatures, J. Geophys. Res., 103(C7), 14,291–14,324, doi:10.1029/ 97JC01444.
675
676 Van Loon H, Rogers J (1978) The Seesaw in Winter Temperatures between Greenland and Northern
677 Europe. Part I: General Description. Monthly Weather Review 106:296-310.
678
679 Van Oldenborgh, G. J., G. Burgers, and A. K. Tank (2000), On the El-Nino teleconnection to spring
680 precipitation in Europe, Int. J. Climat., 20, 565– 574.
681
682 Van Oldenborgh, G. J., and G. Burgers (2005) Searching for decadal variations in ENSO precipitation
683 teleconnections, Geophys. Res. Lett., 32, L15701, doi:10.1029/2005GL023110.
684
685 Vicente-Serrano SM, López-Moreno JI (2008) Nonstationary influence of the North Atlantic Oscillation
686 on European precipitation. J. Geophys. Res., 113(D20), D20120. doi:10.1029/2008JD010382.

687

688 Voldoire, A, Sanchez-Gomez E, Salas y Mélia D, Decharme B., Cassou C., Sénési S., Valcke, S., et al.
689 (2013) The CNRM-CM5.1 global climate model: description and basic evaluation. Clim. Dyn., 40(9-10),
690 2091–2121. doi:10.1007/s00382-011-1259-y

691

692 Wallace JM, Gutzler DS (1981) Teleconnections in the Geopotential Height Field during the Northern
693 Hemisphere Winter. Mon. Wea. Rev., 109, 784–812. doi:10.1175/1520-0493(1981)109.

694

695 Walker G.T (1924) Correlation in seasonal variations of weather, IX. A further study of world weather.
696 Memoirs of the India Meteorological Department, 24, (9) 275-333.

697

698 Wang C. (2002) Atlantic climate variability and its associated atmospheric circulation cells. J. Clim.,
699 15(13), 1516–1536.doi.org/10.1175/1520 0442(2002)015<1516:ACVAIA>2.0.CO;2

700

701 Wang, C, Enfield DB (2003) A Further Study of the Tropical Western Hemisphere Warm Pool. J. Clim.,
702 16, 1476–1493. doi:http://dx.doi.org/10.1175/1520-0442-16.10.1476

703

704 Wang C (2004) ENSO, climate variability and the Walker and Hadley circulations, in The Hadley
705 Circulation: Present, Past and Future, Adv. Global Change Res., vol. 21, edited by H. F. Diaz and R. S.
706 Bradley, pp. 173–202, Springer, New York.

707

708 Wang C, Lee SK, Enfield DB (2008b) Atlantic warm pool acting as a link between Atlantic multidecadal
709 oscillation and Atlantic tropical cyclone activity. Geochem.Geophys. Geosyst. 9 Q05V03. doi:
710 10.1029/2007GC001809.

711

712 Wilks DS (2005) Statistical Methods in the Atmospherics Sciences. Academic Press, 648 pp. ISBN-13:
713 978-0-12-75196.

714

715 Yeh SW, Kirtman BP, Kug JS, Park W, Latif M (2011) Natural variability of the central Pacific El Niño
716 event on multi-centennial timescales. Geophys. Res. Lett., 38(2), n/a–n/a. doi:10.1029/2010GL045886

717

718 Zanchettin D., Franks SW, Traverso P, Tomasino M (2008) On ENSO impacts on European wintertime
719 rainfalls and their modulation by the NAO and the Pacific multi-decadal variability described through the
720 PDO index. Int. J. Climat.28, 995–1006. doi:10.1002/joc.

721

722 Zhang L., Wang C., Wu L (2011) Low-frequency modulation of the Atlantic warm pool by the Atlantic
723 multidecadal oscillation. Clim. Dyn., 39(7-8), 1661–1671. doi:10.1007/s00382-011-1257-0.

724

Figure Captions

Figure 1: a) Leading rainfall empirical orthogonal function over the Euro-Mediterranean region (EOF1, standardized rainfall per standard deviation in the associated PC1) b) 21-years sliding windows correlation between the PC1 and tropical SSTs (5ºS-5ºN) c) Standardized PC1 (blue) and Niño34 (red) Indices. Black boxes in a) indicate the regions used to calculate the rainfall index mentioned in the manuscript (Western Europe minus Western Mediterranean). Statistical significant areas, according to a Monte-Carlo test at the 95% level, are shaded.

Figure 2: Homogeneus (bottom) and heterogeneous (up) regressions maps of respectively SST (º per std. deviation in U) and rainfall (standardized rainfall per standard deviation in U) onto the MCA SST expansion coefficient (U) obtained for N and P periods. On the left (a, c) the leading covariability mode for observed N periods (1944-1964 & 2003-2008) and, on the right (b, d), the same for observed P periods (1900-1940 & 1965-1984).

Figure 3: a) Leading empirical orthogonal function in PICTRL over the Euro-Mediterranean region (EOF1, standardized rainfall per standard deviation in the associated PC1). b) 21-years sliding windows correlation between the interannual rainfall PC1 and the Niño3.4 index (dots), and PC1 of an EOF analysis of the low frequency SSTs (black line, for which only higher periods than 13 years have been considered). Fill dots and shaded areas represent 95% significance according to a Monte-Carlo test.

Figure 4: Same as Fig. 2 but for the long control run in the model CNRM-CM5 (PICTRL).

Figure 5. High (higher that 0.75) minus low (lower that -0.75) composites maps, in N and P periods, based on the first SST MCA standardized expansion coefficient U for a)b) HadISST (º), c)d) Potential velocity (in colour, $10^5 m^2 s^{-2}$), streamfunction (black contours, $ci = 10^6 m s^{-2}$), and divergent wind (arrows, $m s^{-1}$) at 200 hPa, and e)f) Sea Level Pressure (Pa). Statistical significant areas, according to a Monte-Carlo test at the 95% level, are shaded. In figures 5c-d only the 95% significant streamfunction is contoured (being solid lines positive values and dashed lines negative ones).

Figure 6: Same as Fig. 5 but for the long control run in the model CNRM-CM5 (PICTRL). Here, higher values than 1 (U>1 standard deviation) and lower values than -1 (U<-1 standard deviation) have been considered for the composites maps.

Figure 7: Same composites maps of streamfunction (shaded; $10^7 m s^{-2}$) as in a) Figure 6c, b) Figure 6d, and c) Figure 5d. In contours the zonal mean flow at 200 hPa (contours, ci= $5 m s^{-2}$), being the maximum and minimum value represented 10 and 50 $m s^{-2}$ in each case.

761 Figure 8: High (P periods) minus low (N periods) significant composites maps in PICTRL for a) zonal
762 mean flow at 200 hPa (ms^{-2}), b) mean squared Rossby wavenumber at 200 hPa (Ks2) and c) SST (^{o}).
763 The climatological zonal mean flow (a) and the climatological mean squared Rossby wavenumber (b) at
764 200 hPa are also shown in contours levels, being the maximum and minimum value represented 20 and
765 50 ms^{-2} (ci= $5\,ms^{-2}$) in the former case, and 10 and 50 (ci=5) in the latter case. Only the 90 %
766 statistical significant areas, according to the Wilcoxon-Mann-Whitney test, are plotted.

Figure

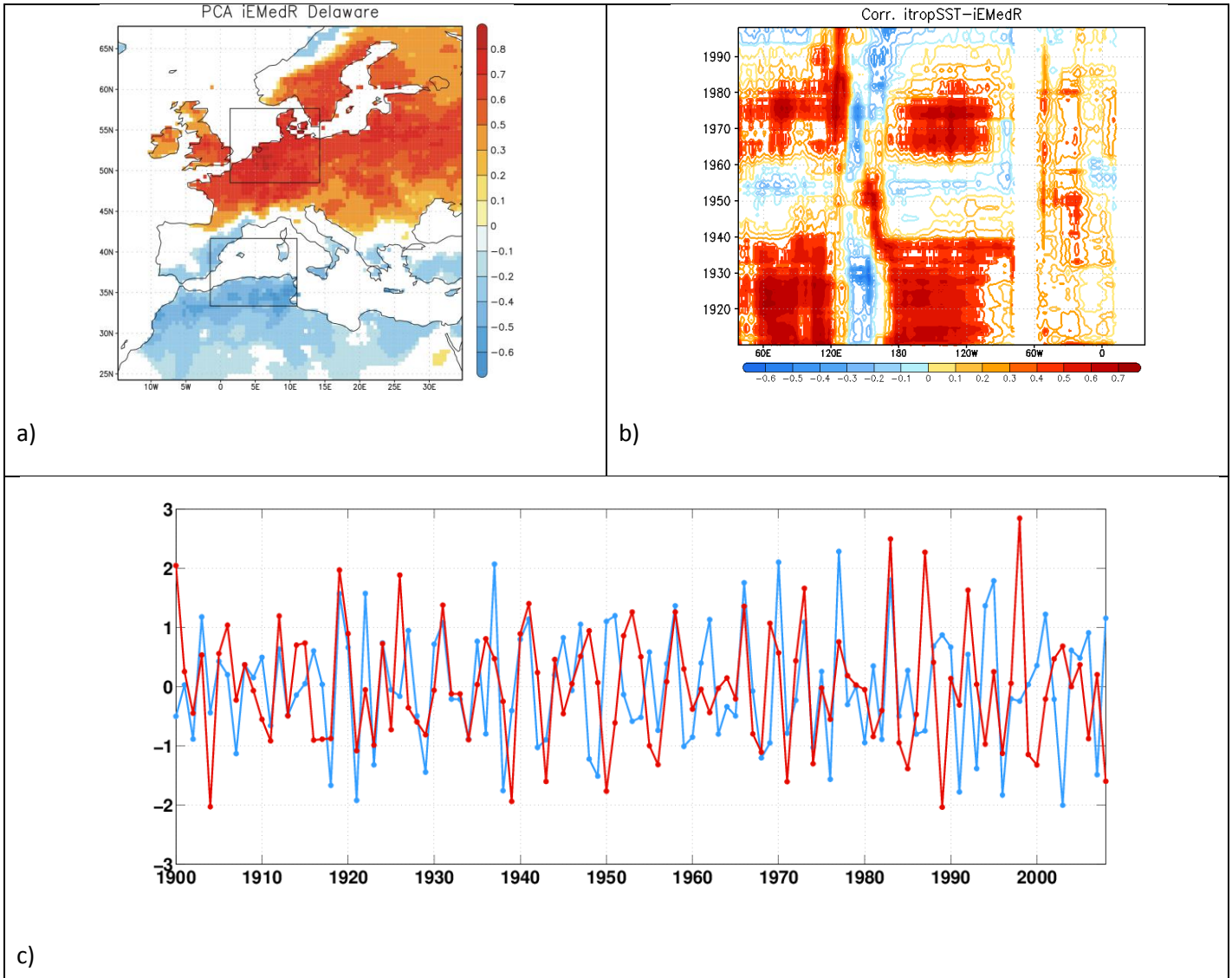

Figure 1. a) Leading rainfall empirical orthogonal function over the Euro-Mediterranean region (EOF1, standardized rainfall per standard deviation in the associated PC1) b) 21-years sliding windows correlation between the PC1 and tropical SSTs (5ºS-5ºN) c) Standardized PC1 (blue) and Niño34 (red) Indices. Black boxes in a) indicate the regions used to calculate the rainfall index mentioned in the manuscript (Western Europe minus Western Mediterranean). Statistical significant areas, according to a Monte-Carlo test at the 95% level, are shaded.

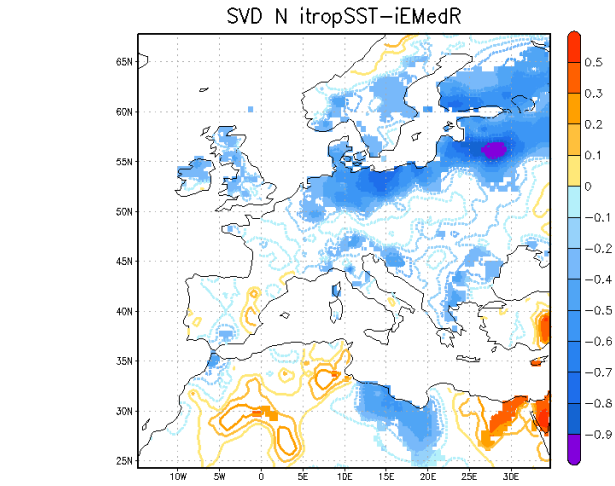

a)

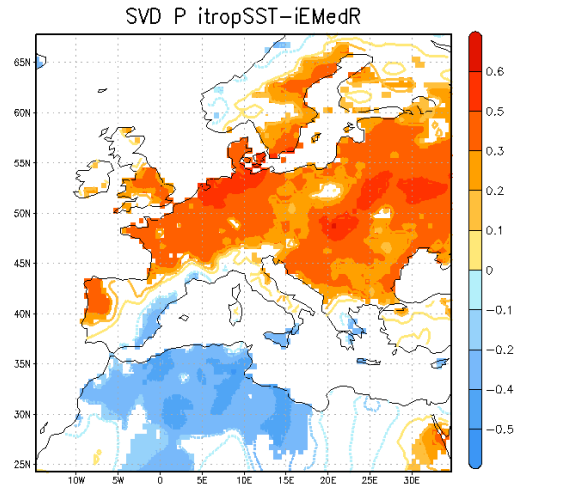

b)

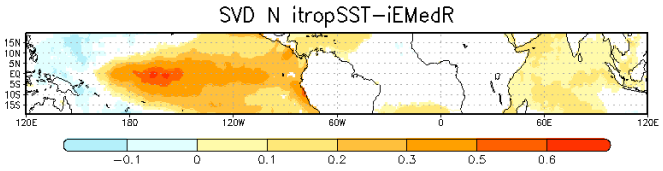

c)

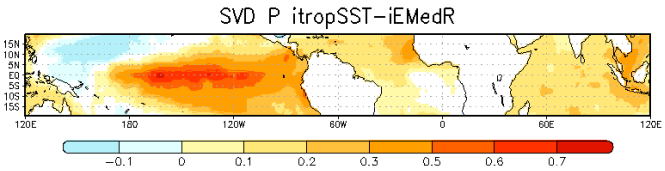

d)

Figure 2. Homogeneus (bottom) and heterogeneous (up) regressions maps of respectively SST (º per std. deviation in U) and rainfall (standardized rainfall per standard deviation in U) onto the MCA SST expansion coefficient (U) obtained for N and P peridos. On the left (a, c) the leading covariability mode for observed N periods (1944-1964 & 2003-2008) and, on the right (b, d), the same for observed P periods (1900-1940 & 1965-1984).

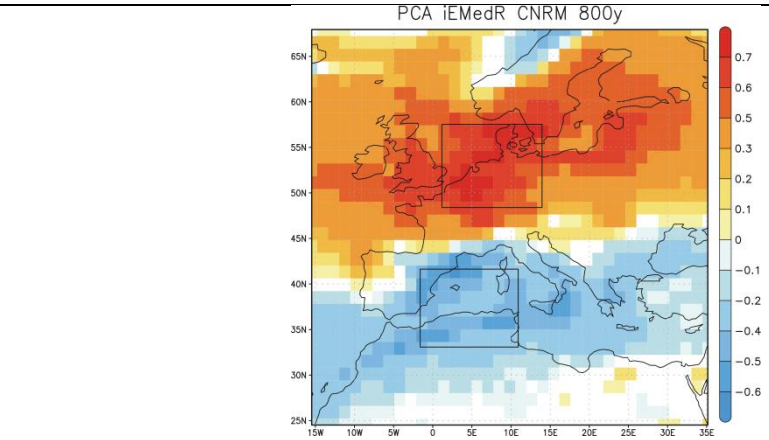

a)

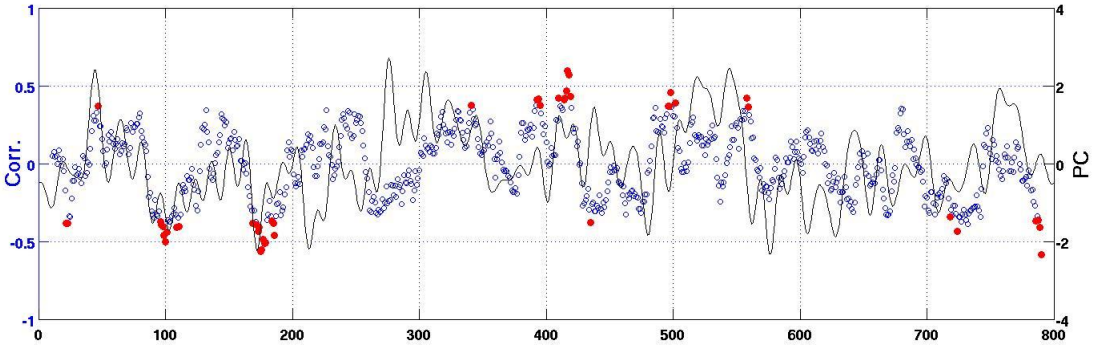

b)

Figure 3. a) Leading empirical orthogonal function in PICTRL over the Euro-Mediterranean region (EOF1, standardized rainfall per standard deviation in the associated PC1). b) 21-years sliding windows correlation between the interannual rainfall PC1 and the Niño3.4 index (dots), and PC1 of an EOF analysis of the low frequency SSTs (black line, for which only higher periods than 13 years have been considered). Fill dots and shaded areas represent 95% significance according to a Monte-Carlo test.

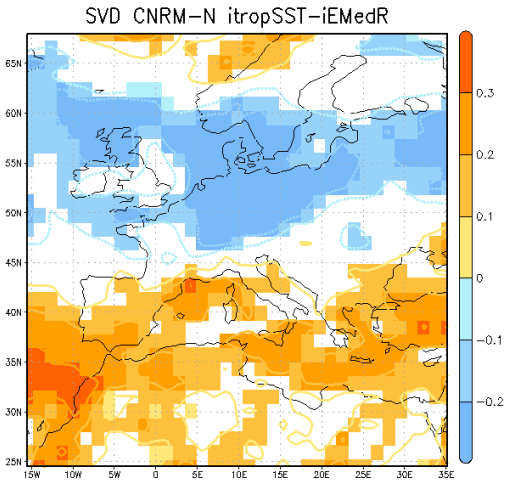

a)

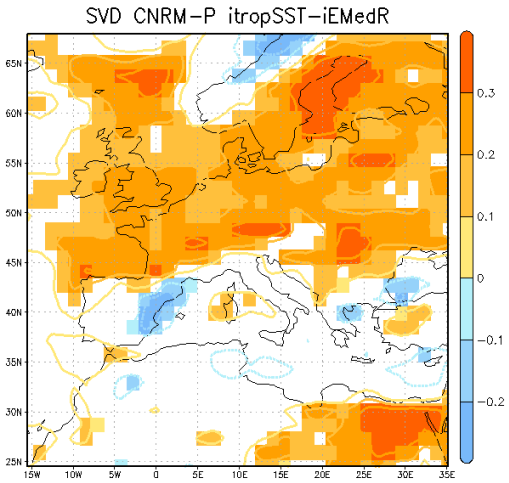

b)

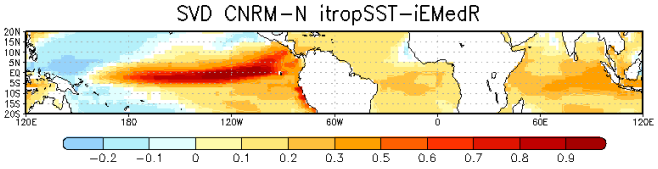

c)

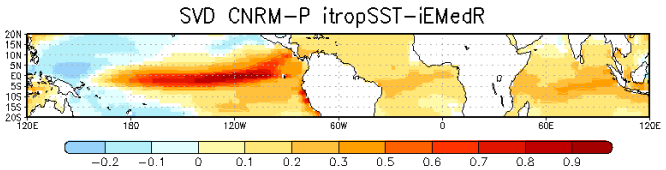

d)

Figure 4. Same as Fig. 2 but for the long control run in the model CNRM-CM5 (PICTRL).

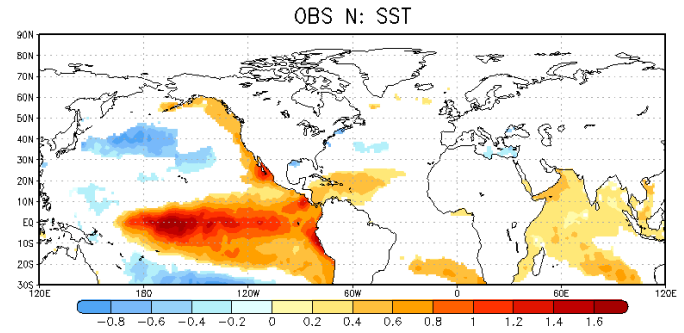

a)

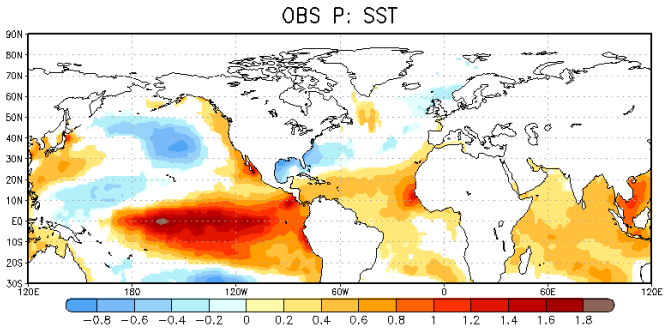

b)

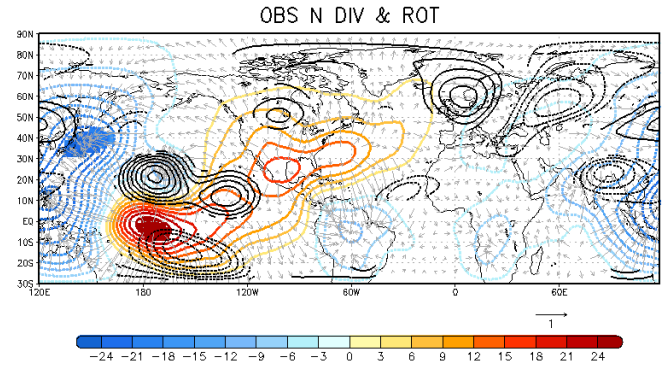

c)

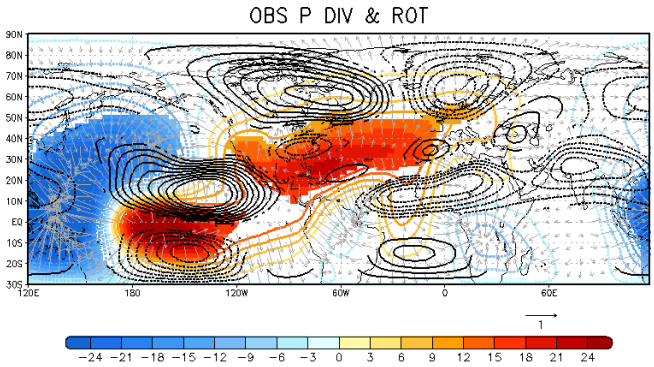

d)

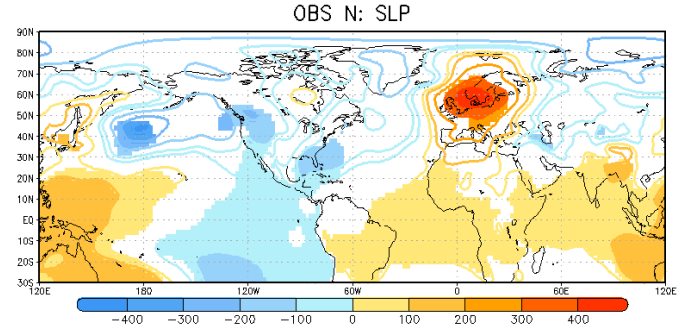

e)

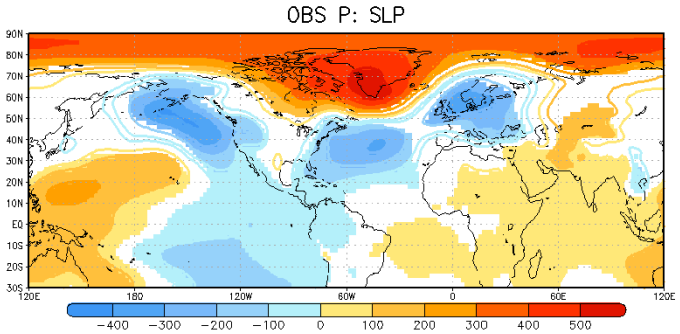

f)

Figure 5. High (higher than 0.75) minus low (lower than -0.75) composites maps, in N and P periods, based on the first SST MCA standardized expansion coefficient U for a)b) HadISST (º), c)d) Potential velocity (in colour, $10^5 m^2 s^{-2}$), streamfunction (black contours, $ci = 10^6 m s^{-2}$),

and divergent wind (arrows, ms^{-1}) at 200 hPa, and e)f) Sea Level Pressure (Pa). Statistical significant areas, according to a Monte-Carlo test at the 95% level, are shaded. In figures 5c-d only the 95% significant streamfunction is contoured (being solid lines positive values and dashed lines negative ones).

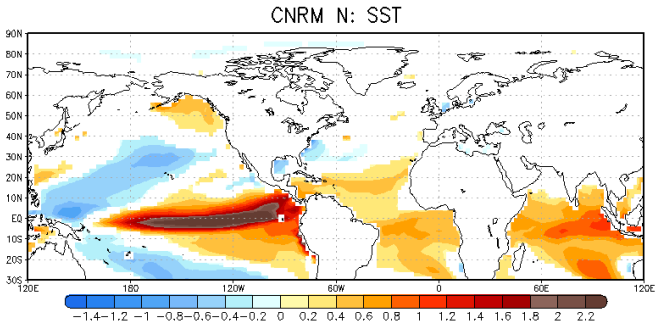

a)

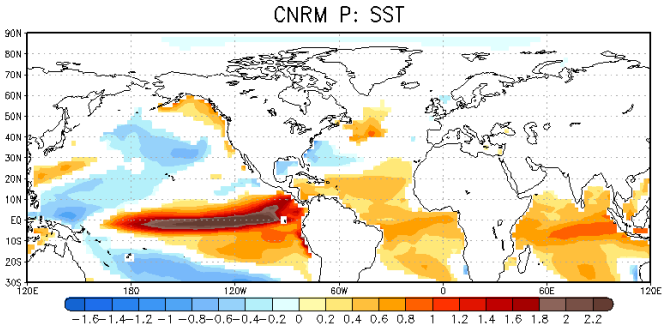

b)

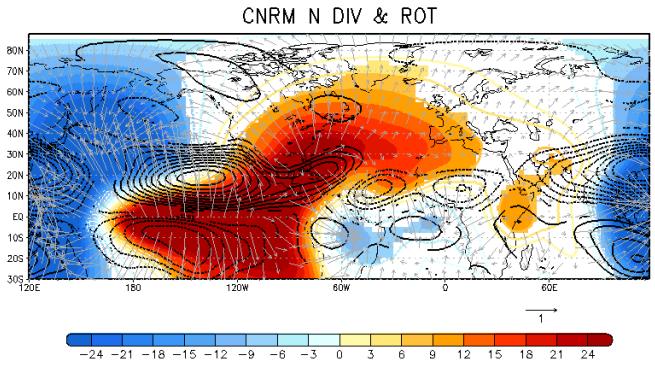

c)

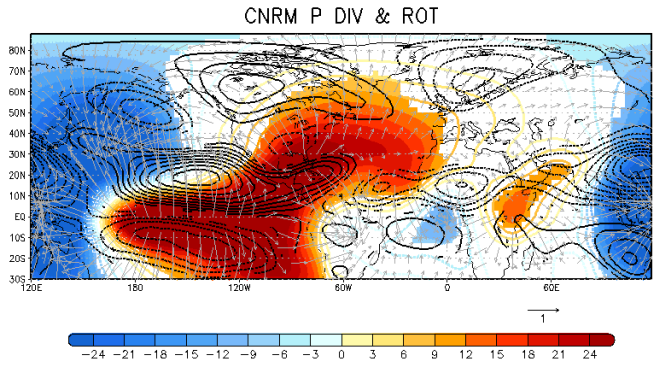

d)

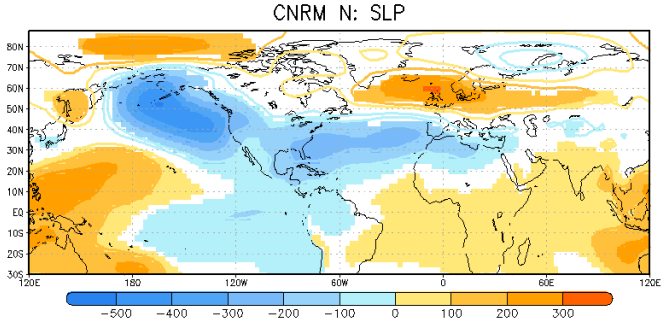

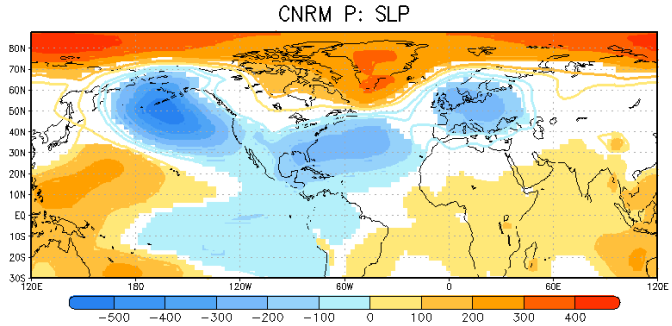

e)	f)

Figure 6. Same as Fig. 5 but for the long control run in the model CNRM-CM5 (PICTRL). Here, higher values than 1 (U>1 standard deviation) and lower values than -1 (U<-1 standard deviation) have been considered for the composites maps.

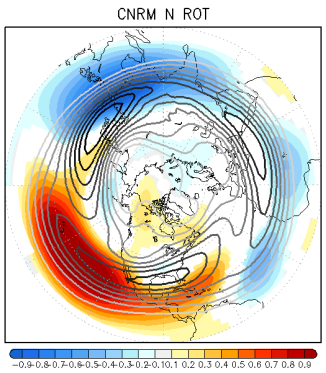

a)

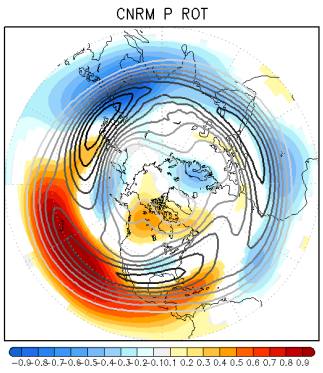

b)

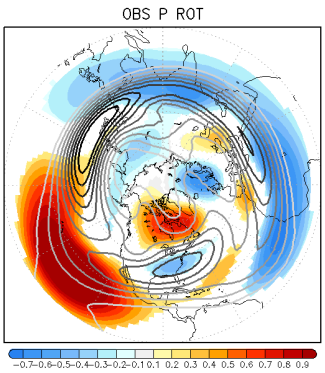

c)

Figure 7: Same composites maps of streamfunction (shaded; $10^7\, m\, s^{-2}$) as in a) Figure 6c, b) Figure 6d, and c) Figure 5d. In contours the zonal mean flow at 200 hPa (contours, ci= 5 $m\, s^{-2}$), being the maximum and minimum value represented 10 and 50 $m\, s^{-2}$ in each case.

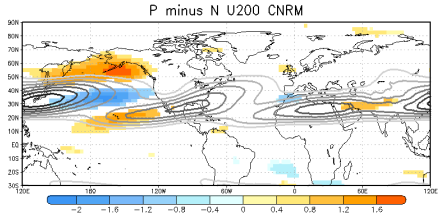

a)

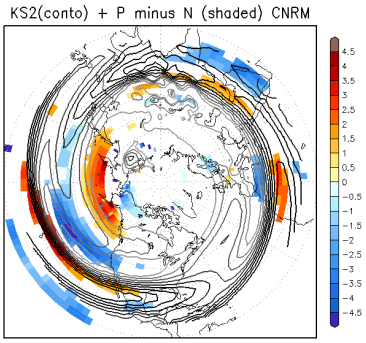

b)

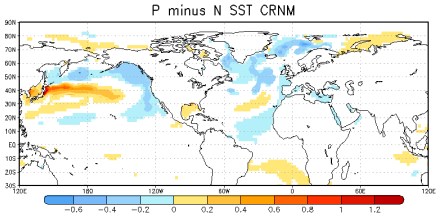

c)

Figure 8. : High (P periods) minus low (N periods) significant composites maps in PICTRL for a) zonal mean flow at 200 hPa ($m\, s^{-2}$), b) mean squared Rossby wavenumber at 200 hPa (Ks2) and c) SST (º). The climatological zonal mean flow (a) and the climatological mean squared Rossby wavenumber (b) at 200 hPa are also shown in contours levels, being the maximum and minimum value represented 20 and 50 $m\, s^{-2}$ (ci= 5 $m\, s^{-2}$) in the former case, and 10 and 50 (ci=5) in the latter case. Only the 90 % statistical significant areas, according to the Wilcoxon-Mann-Whitney test, are plotted.

Electronic Supplementary Material

Click here to download Electronic Supplementary Material: ad.material.docx